Non-Equilibrium Carrier Transport in Strongly Coupled Quantum Dot Solids and Heterostructures

Mengxia Liu,[1] Sachin Dev Verma,[1,2] Zhilong Zhang,[1] Jooyoung Sung,[1*] Akshay Rao[1*]

[1]*Cavendish Laboratory, University of Cambridge, JJ Thomson Avenue, Cambridge CB3 0HE, United Kingdom*

[2]*Department of Chemistry, Indian Institute of Science Education and Research Bhopal, Bhopal Bypass Road, Bhopal 462066, Madhya Pradesh, India*

*Correspondence and requests for materials should be addressed to Jooyoung Sung (Email: js2377@cam.ac.uk), or Akshay Rao (Email: ar525@cam.ac.uk)

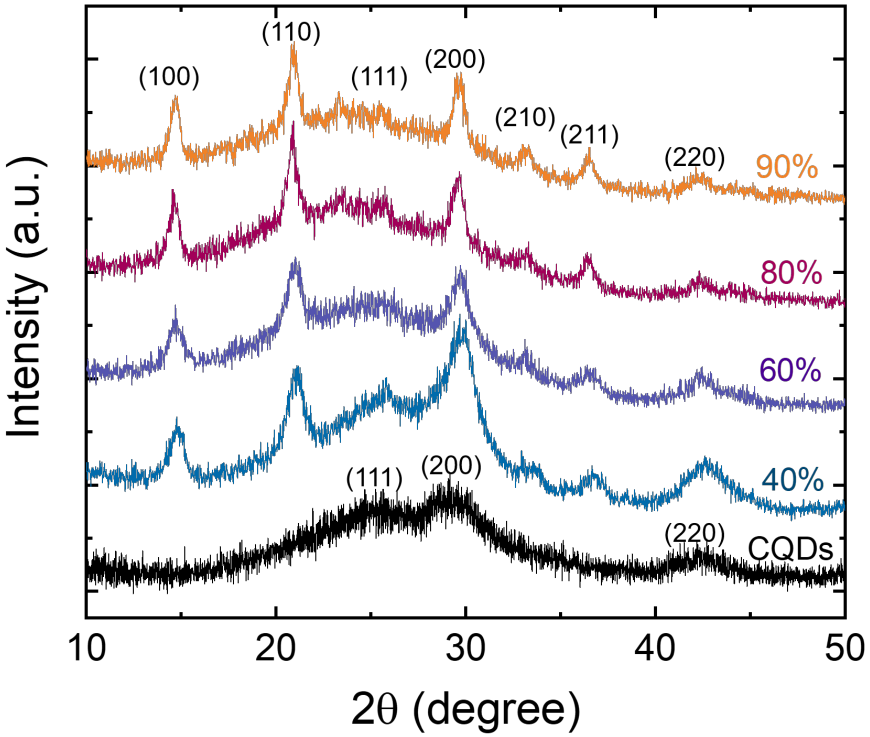

Supplementary Figure 1. X-ray diffraction of the CQD:$CsPbBr_2I$ films. The different curves correspond to different perovskite volume percentages as labelled. The black curve represents the XRD pattern for pure CQD film. The $CsPbBr_2I$ and PbS show strong agreement in the lattice parameter, suggesting an ideal lattice matching between the perovskite matrix and embedded CQDs.

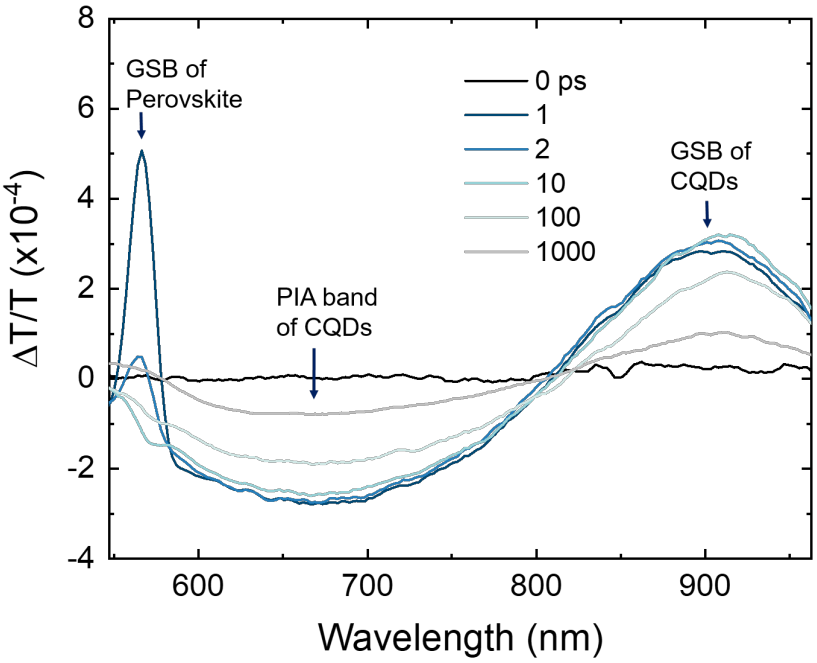

Supplementary Figure 2. Transient absorption spectra of QDiP solids (perovskite volume percentage is 60%) taken at different time delays. A pump photon energy of 2.34 eV is used to excite both perovskite matrix and embedded dots.

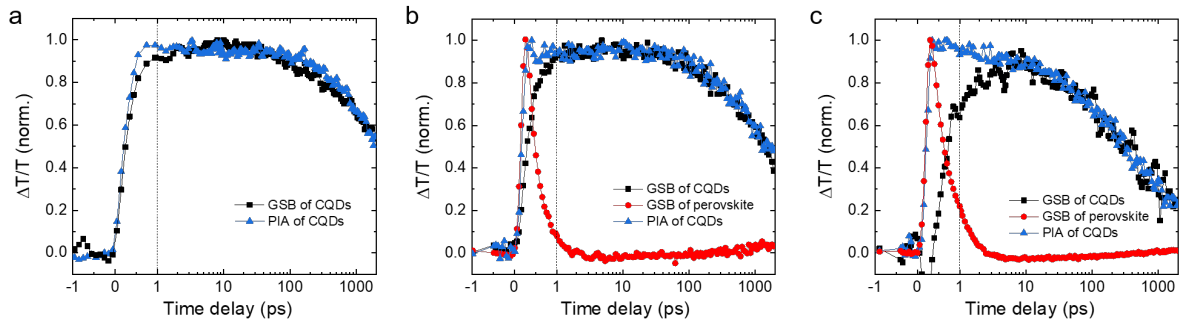

Supplementary Figure 3. Time traces for the pure CQD solids (a), PiQD solids with 40 vol% perovskite (b), and PiQD solids with 60 vol% perovskite (c). For QDiP solids, the kinetics probed at each GSB peak suggests a carrier transfer process from perovskite to CQDs. The PIA band of CQDs is insensitive to the injected carriers and the decay traces correspond to the carrier recombination in CQDs. The decay rate at PIA peak for different samples are not identical. As perovskite content increases, embedded dots exhibit stronger Auger recombination as CQDs become overloaded with carriers injected from surrounding perovskite.

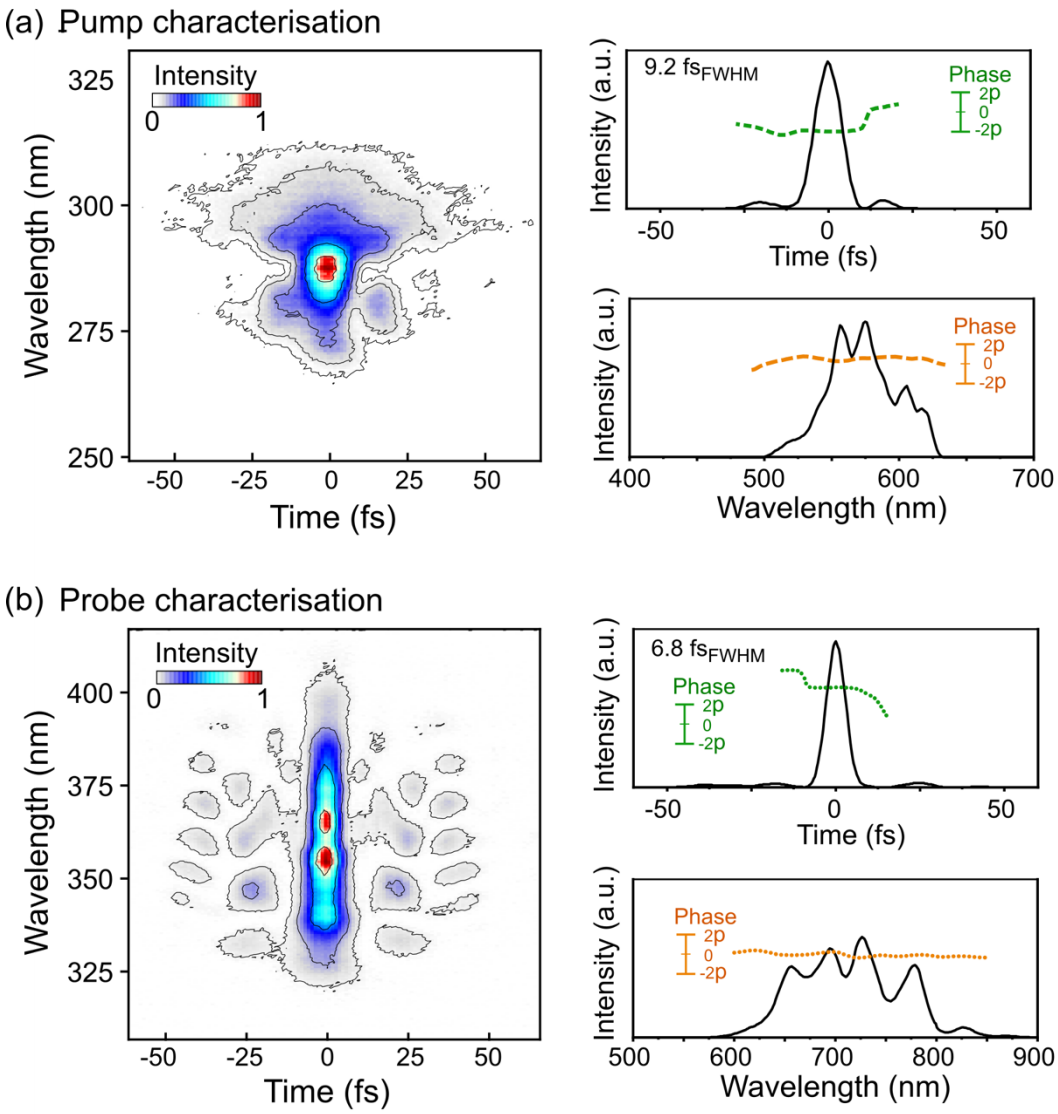

Supplementary Figure 4. (a) Pump pulse characterisation. Left: SHG-FROG trace of pump obtained after compression. Top right: temporal profile (black solid line) and phase (green dotted line) retrieved from the SHG-FROG trace of pump. Bottom right: the SHG-FROG spectrum (black solid) and phase (orange dotted line), retrieved from the SHG-FROG trace of pump. (b) Probe pulse characterisation. Left: SHG-FROG trace of probe obtained after compression. Top right: temporal profile (black solid line) and phase (green dotted line) retrieved from the SHG-FROG trace of probe. Bottom right: the SHG-FROG retrieved spectrum (black solid) and phase (orange dotted line), retrieved from SHG-FROG trace of pump.

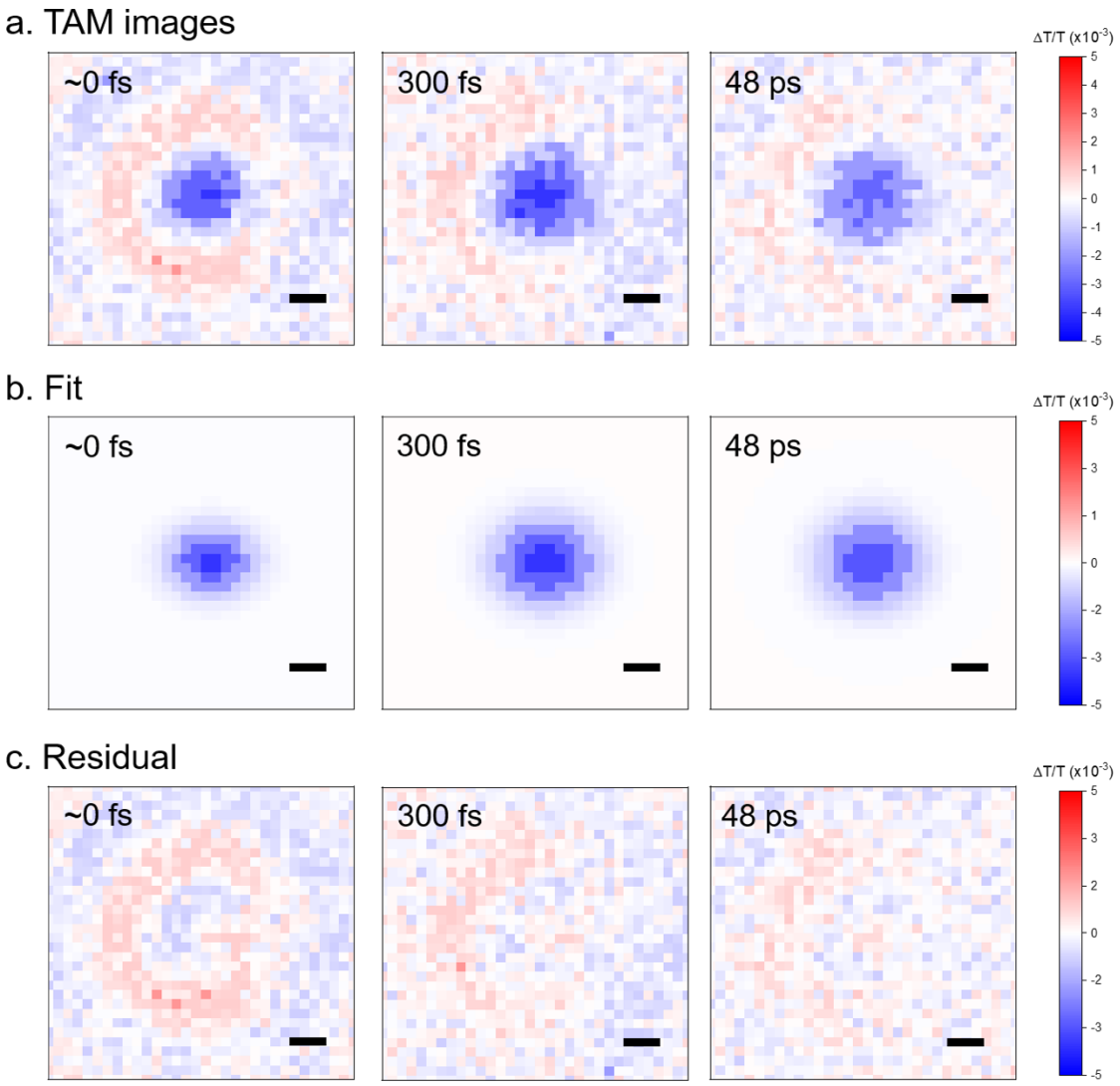

Supplementary Figure 5. (a) Representative TAM images of pure CQD solids obtained at 690 nm. (b) The corresponding fit images simulated by 2D Gaussian functions. (c) The residual of fits. Scale bars, 200 nm.

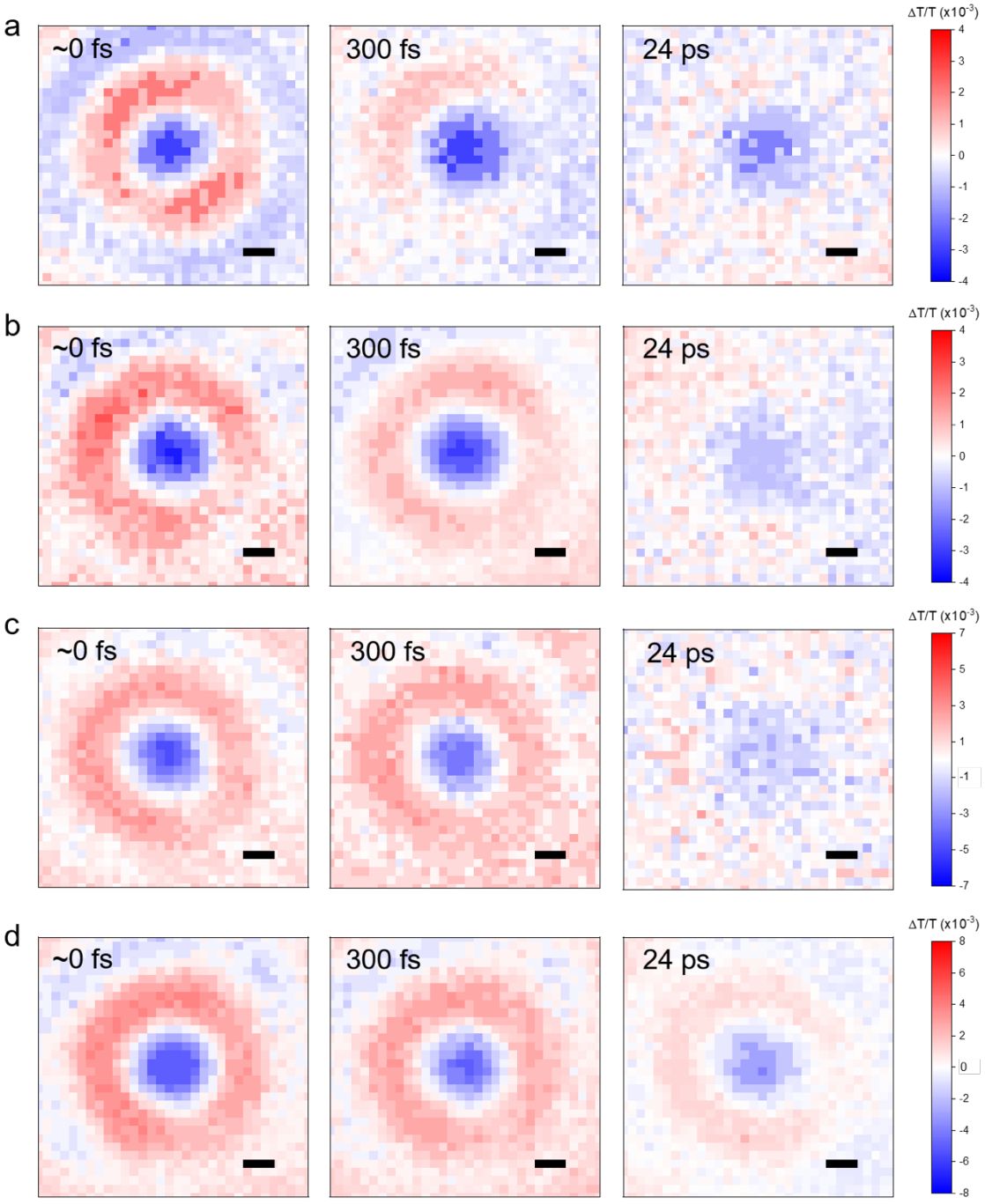

Supplementary Figure 6. Representative TAM images of QDiP solids with a perovskite loading of 40 vol% (a), 60% (b), 80% (c), and 90% (d). Scale bars, 200 nm.

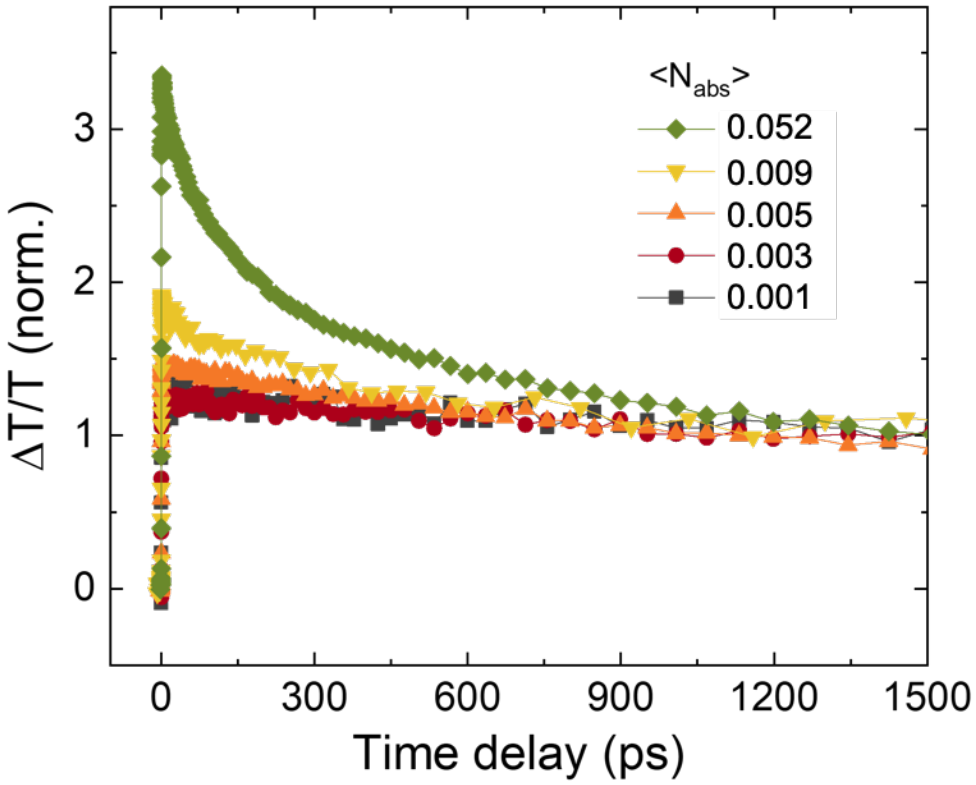

Supplementary Figure 7. Time traces for the pure CQD solids measured at different excitation intensity. The fast, higher-order Auger recombination process occurs at high excitation intensities.

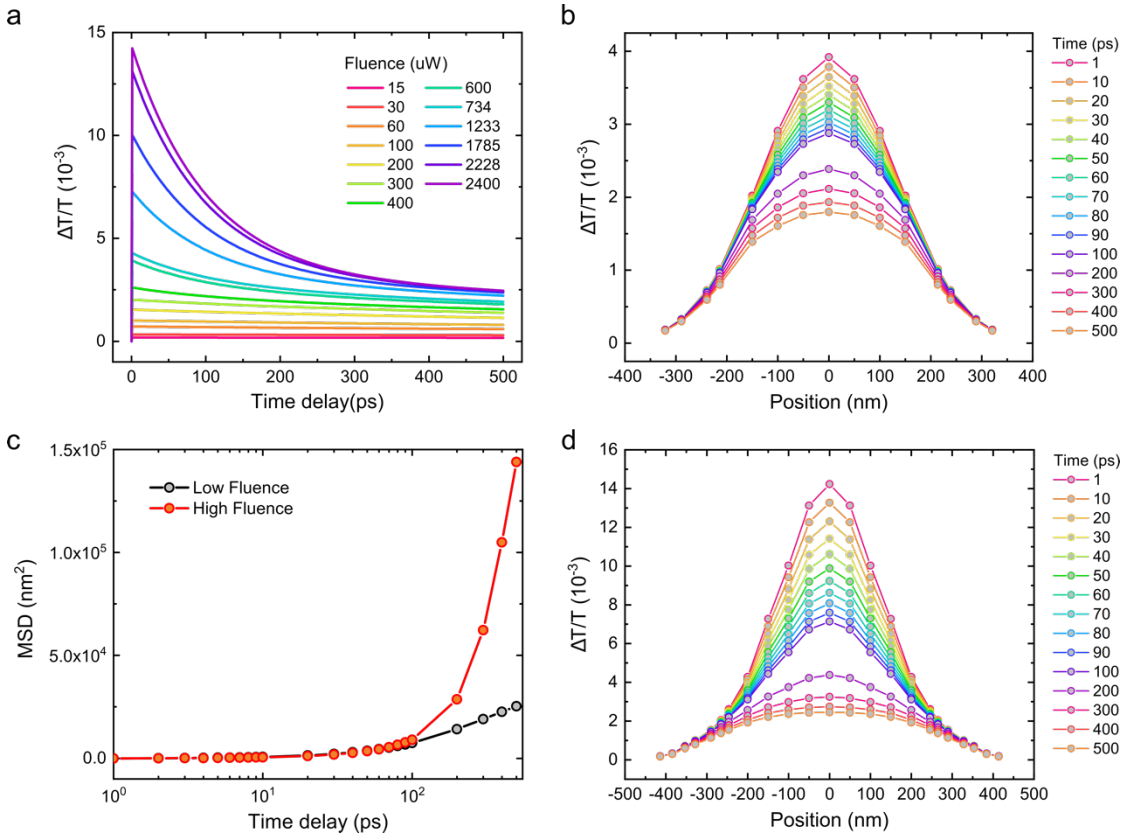

Supplementary Figure 8. Simulation results for false expansion caused by carrier-carrier annihilation. (a) Simulated fluence-dependent TA kinetics. (b) and (d) Simulated carrier densities at different time delays under low pump fluence, $\langle N_{abs} \rangle = 0.045$ (b), and high pump flunece, $\langle N_{abs} \rangle = 0.18$ (d). (c) Simulated time-evolution of mean-square-displacement caused solely by carrier-carrier annihilation. The simulated result shows that carrier-carrier annihilation leads to false expansion under both pump fluences. Within 100 ps, the false expansion values for low and high fluences are similar.

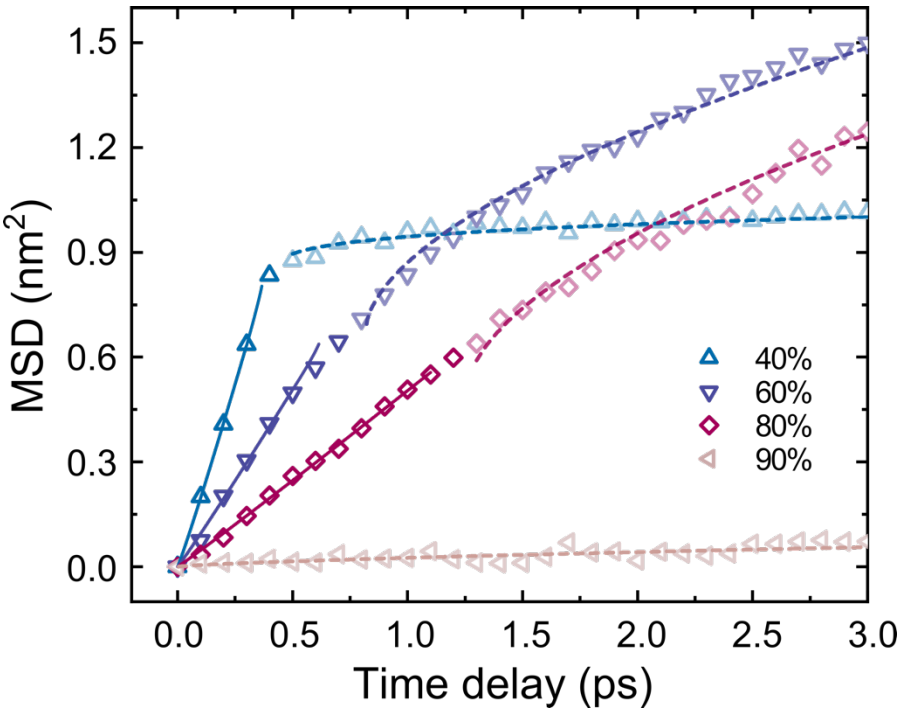

Supplementary Figure 9. Initial temporal evolution of MSD for QDiP solids. The different curves correspond to different perovskite volume percentages, as labelled. Experimental values are displayed as symbols. The solid lines are the linear fits for the band-like regime, following the equation $MSD(t) = 2Dt$, where D is diffusivity. The dashed lines are sublinear fits for the hopping regime following the equation $MSD(t) = MSD(t_{band-like}) + A(t - t_{band-like})^{\alpha}$, where A is a proportionality factor with fractional time units, α is the diffusion exponent, and $t_{band-like}$ represents the persisting time of band-like regime. We note that fitting only the first regime with $2Dt^{\alpha}$ yields almost identical D values and α values of around 1. After the completion of band-like transport, the samples with higher perovskite content exhibit a higher carrier hopping rate. This is attributed to the stronger Auger recombination processes in CQDs as the CQDs become overloaded with carriers from the surrounding carrier-donor matrix.

Supplementary Note 1. The effect of Auger recombination on time-evolution of carrier distribution.

Charge carriers in colloidal quantum dots (CQDs) undergo Auger recombination process upon excess carrier generation. The transient absorption kinetic profiles of our tested systems (CQD and QDiP solids) show clear characteristic of Auger recombination at $<N_{abs}>$ higher than 0.005 (Supplementary Fig. 7).

In TAM measurements, the excited carrier distribution resembles the shape of the pump pulse, resulting in a higher carrier density at the centre of the spot compared to the edge. Under excitation intensities taken for our TAM studies ($<N_{abs}>$ = 0.045, 0.09, 0.18), Auger recombination is prominent. Carriers undergo radiative decay and diffusion, but additionally annihilate with a rate that depends nonlinearly on the local carrier density. The spatially varied carrier dynamics leads to artificial flattening and broadening of σ.

To correctly analyse the effect of Auger process on carrier transport, we simulated the distribution broadening resulted from spatially varied carrier dynamics alone, leaving diffusion process out of account. The simulation protocol is briefly described as follows. First, we estimate the initial carrier densities at different positions based on the excitation power and dT/T intensity at specific positions. The fluence-dependent kinetic profiles obtained from conventional TA measurement (Supplementary Fig. 7) were used as the main data set, and the missing kinetics at various fluences were generated by fitting with three exponential decay function (Supplementary Fig. 8a). The simulated TA profiles are well matched with the recorded TA profiles, indicative of high reliability for the simulation of fluence-dependent TA kinetics. Second, we generated three-dimensional data sets (x (position or carrier density), y (dT/T), z (time)), reshaped them into 1D-TAM profile and plotted them as a function of time, as shown in Supplementary Fig. 8b and 8d. Finally, by fitting the 1D-TAM profile with 1D-Gassuain functions we obtained the MSD profiles as shown in Supplementary Fig. 8c.

The MSD profiles simulated at low and high pump fluences ($<N_{abs}>$ = 0.045 and 0.18, respectively) reveal no pronounced difference in artificial broadening up to 100 ps. In sharp contrast, the experimentally obtained MSD profiles demonstrate positive scaling of MSD with increasing fluence (Figure 3a and 3b). We therefore assign this phenomenon to the spatial motion of Auger-assisted carriers with excess energy.